

Modelling the effects of Concentrated Emissions Sources on Tropospheric Ozone

J.D.B. Smith¹ (joels@chem.leeds.ac.uk), A.S. Tomlin², M. Berzins³, V. Pennington³, and M.J.Pilling¹

¹ School of Chemistry, University of Leeds, Leeds, LS2 9JT UK

² Dept. of Fuel and Energy, University of Leeds, Leeds, LS2 9JT UK

³ School of Computer Studies, University of Leeds, Leeds, LS2 9JT UK

1. Abstract

This paper briefly describes current work on the use of adaptive grid techniques applied to an atmospheric chemistry problem. The use of these techniques in atmospheric reactive flow problems has recently been described by Tomlin *et al.*[1], using a single point source in a region of uniform fixed emissions. The work of that paper has been extended to incorporate emissions based on UK inventories and two different chemical schemes.

2. Introduction

Ozone concentrations in the atmospheric boundary layer, the bottom kilometre of the troposphere, are dependent on the interactions of nitrogen oxides and the volatile organic compounds (VOCs) that are emitted from both anthropogenic and biogenic sources. For regional air pollution models the aim is to have high spatial resolution, combined with as detailed chemical schemes as possible, to help in fully understanding all the complex processes occurring in the troposphere, but this aim has not been achieved so far.

Some models have used 1-D Lagrangian trajectory representations[2] of the reactive flow problem which enabled the inclusion of large chemical schemes, as do coarse Eulerian meshes. These models have helped to improve our understanding of the complex chemical processes that lead to build up of secondary pollutants, such as ozone. However, mixing processes are poorly described in these forms of model, so the effects of concentrated emission sources, such as power stations, tend to be underplayed through averaging over a larger area. Other models have used high resolution meshes but have used greatly simplified chemical schemes, which do not enable the analysis of the impact of individual chemical species on the pollutant distribution.

Telescopic grids have been viewed[3-6] as one way of incorporating larger chemical schemes, while still providing sufficient spatial resolution around high emission point sources. By placing the larger mesh elements downwind of the emission sources it was hoped to avoid unnecessarily detailed calculations where they weren't justified. However, large spatial gradients in pollutant concentrations still exist in plumes that are hundreds of kilometres downwind of their source. When the plume enters a large mesh element, the solution becomes 'smeared' by averaging, which provides inaccurate downwind profiles.

Tomlin *et al.*[1,7] recently demonstrated the use of time-dependent adaptive mesh gridding techniques applied to the investigation of a single power station plume, with regards to regional ozone levels. The results of that paper highlighted the differences in the total and peak concentrations of ozone arising from using fixed meshes, as opposed to using adaptive mesh gridding techniques.

This paper investigates the effects of multiple point sources interacting with the more diffuse area sources arising from urban emissions. The numerical code, SPRINT2D[8], provides spatial and temporal error controls for limiting the adaptation of the mesh for length scales ranging from a few hundred metres to a few hundred kilometres.

3. Model & Methodology

The model, as shown in Figure 1, describes the emissions from power stations, as well as the more diffuse emissions from urban areas, using the atmospheric diffusion equation in two space dimensions.

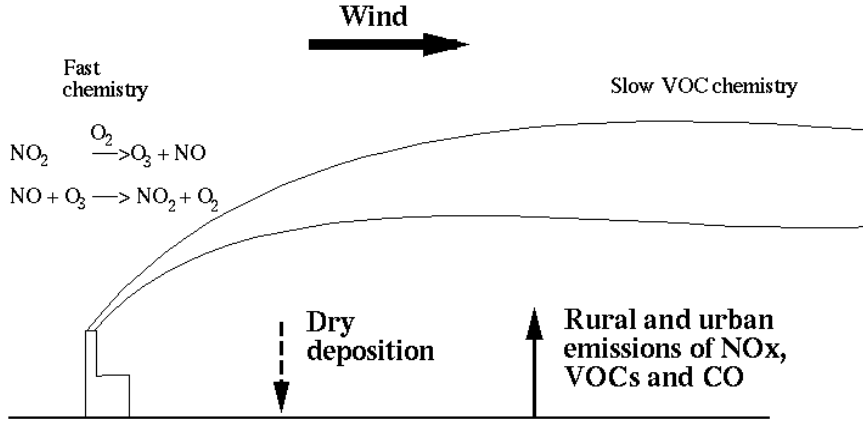


Figure 1. Schematic diagram of the model

3.1 Model equations

$$\begin{aligned} \frac{\partial c_s}{\partial t} = & -\frac{\partial u c_s}{\partial x} - \frac{\partial w c_s}{\partial y} + \frac{\partial}{\partial x} \left(K_x \frac{\partial c_s}{\partial x} \right) + \frac{\partial}{\partial y} \left(K_y \frac{\partial c_s}{\partial y} \right) \\ & + R_s(c_1, c_2, \dots, c_q) + E_s - (\kappa_{1s})c_s \end{aligned} \quad (1)$$

where c_s is the concentration of the s 'th compound, u, w are wind velocities in the x and y directions, K_x and K_y are turbulent diffusivity coefficients, κ_{1s} is a dry deposition velocity, E_s describes distribution of emission sources for s 'th compound, and R_s is the chemical reaction term which may contain nonlinear terms in c_s . This produces, for n chemical species, an n -dimensional set of partial differential equations (p.d.e.s) that describe the rate of change of the concentration of the chemical species with respect to time and space. These equations are coupled through the nonlinear chemical reaction terms.

3.2 Numerical Methods

The numerical methods used are described in more detail in Tomlin *et al.*, [1] Berzins *et al.* [8-12] but a brief summary of the main points is given here.

3.2.1 Spatial discretisation. Unstructured triangular meshes are favoured by finite volume/element practitioners for their ability to deal with general two dimensional geometries. Although the domain under investigation is of a regular nature, the complex structures arising from the interactions between the point sources and large area sources are better resolved using this form of mesh. The atmospheric diffusion equation was used to produce a set of p.d.e.s which are discretised in space on to the unstructured triangular mesh. This converts the set of p.d.e.s in three independent variables into a set of ordinary differential equations (o.d.e.s) in one independent variable, time. The spatial discretisation used was based on a triangular finite volume approach [12], whereby the solutions are represented, using the 'method of lines', as a series of piecewise constant elements. A cell centred scheme was used, wherein the p.d.e. is integrated across the triangular element and the divergence theorem applied, to convert the area integral into a line integral over the three edges. In order to reduce the line integrals into flux evaluations at the midpoint of each edge, the midpoint quadrature rule was used.

The second order approximate Riemann solver of Berzins and Ware [12] was used to calculate the flow between the elements, since this will tend to reduce the numerical diffusion in the solution and preserves steep spatial gradients. Steep concentration gradients can occur in the vicinity of concentrated emissions sources, as well as a long way downwind, so this second order solver helps achieve a more accurate representation. The solver was only applied to the advective terms, while a central differencing method was used for the diffusive terms.

3.2.2 Time integration and operator splitting. Having discretised the p.d.e. system in space, the resulting coupled o.d.e. system was of size $m \times n$, where m was the number of triangles in the initial mesh and n was the number of chemical species. The o.d.e system was solved as an initial value problem, utilising the modified Theta method[13] and functional iteration to solve the large system of non-linear equations. With the two chemical schemes described later, this gave initial system sizes of 5000 and 23000 o.d.e.s, the solution of which takes the majority of the computational time.

To reduce the computational overhead, a form of operator splitting was used that was based on the decomposition of the p.d.e.s into a set of flow terms and a set of reactive source terms. The implementation of this is detailed in Tomlin *et al.*[1], so it is simply worth noting that this produces a speed-up factor of between five and ten, when compared with the Newton-Krylov method used previously.

3.2.3 Adaptivity. The initial mesh was created using the Geompack[14] mesh generator, which is very flexible and capable of taking any geometric input file prior to producing the mesh. There exists the capability to pre-refine the mesh around the most concentrated sources of interest, a form of telescoping the mesh, which produces mesh elements of about 800 – 900 metres along the longest edge, whereas the larger mesh elements will be of around 20 – 30 kilometres. This ensures that in the initial stages of the calculations the steep gradients are preserved.

Once the simulation was started, for each element a spatial error estimate for the next time step was made. If this error was larger than some predefined value, then local h-refinement will occur, which produces mesh elements that are of the same quality as the original, larger elements. All hanging nodes are removed by bisecting the neighbouring triangle. Should an element be later marked for derefinement, the data structure exists such that the original larger elements are reformed by removal of the inner element. The maximum number of times an element can be refined was stipulated at the start of the calculation to prevent excessive refinement around concentrated sources. The combination of both absolute and relative error controls provided by SPRINT2D means that quite sophisticated manipulation of the calculations can take place. The mesh refinement was dictated by spatial errors in the concentration of NO, although similar results arise from using ozone as the monitored species.

3.3 Model Inputs and Parameterisations

The diurnal variations of the temperature, relative humidity, solar zenith angle and mixing layer height were all parameterised according to [15]. The photochemical reaction rates, in the form $J = a_i \exp(-b_i \sec(\theta))$, were dependent on the solar zenith angle (θ), which varied as a function of the local time (LHA = local hour angle), time of year (DEC = solar declination angle) and latitude (LAT).

$$\cos(\theta) = \cos(\text{LHA})\cos(\text{DEC})\cos(\text{LAT}) + \sin(\text{DEC})\sin(\text{LAT}) \quad (2)$$

The values used for DEC and LAT in this study were for July at 50 degrees N. The temperature dependent rate constants were given in their normal Arrhenius form, with the diurnal temperature cycle being given by

$$T/\text{K} = 289.86 + 8.3\sin((7.27 \times 10^{-5}t) - 1.96) \quad (3)$$

The mixing layer height changes between 300 and 1300 metres, starting to increase two hours after dawn, and reaching its maximum at 15:00 each day before returning to the lower level overnight. The mixing height affects the rates of emission and deposition of the various species in this bottom region of the troposphere.

The emissions data come from the UK National Atmospheric Emissions Inventory (NAEI), which gives annual totals for carbon monoxide, nitrogen oxides (NO + NO_x) and non-methane VOCs (NMVOCs) broken down into 10km × 10km grid squares, using the UK Ordnance Survey (OS) map coordinates. Point sources are included separately from the disaggregated urban emissions, but for confidentiality reasons the exact placements of industrial plants were not included, so these data were incorporated with the disaggregated inventory. Power stations are listed separately as NO_x point source emitters, with 90% of the emitted total being in the form of NO, while the rest is taken to be NO₂. The emissions data were interpolated from a base mesh onto the triangular calculation mesh whenever the mesh was refined. Although the mechanism for the inclusion of variable wind speed and direction was in place, the results shown were for a fixed wind speed in one direction.

4. Chemical schemes

In the initial stages of this project, a reduced chemical mechanism was used that had formaldehyde as a representative volatile organic compound (VOC). This work includes two more rigorously tested chemical mechanisms, to try and compare their effectiveness for predicting regional ozone levels. The first, the Generic Reaction Set, was formulated by Azzi *et al.*[16], while the second scheme, known hereafter as CBMLeeds[17], was the result of a systematic reduction of the Extended Carbon Bond (CBM-Ex) mechanism of Gery *et al.*[18].

4.1 The Generic Reaction Set (GRS)

The GRS consists of seven species and seven reactions, with NO, NO₂ and ozone being the only true chemical species used. The remaining four are surrogate species. The scheme was created by fitting experimental smog chamber data to provide a compact scheme that could model photochemical smog. It has been utilised successfully by Venkatram *et al.*[19] in their Regional Ozone Decision Model, and has been shown to model peak ozone concentrations with an accuracy comparable to more detailed schemes, although it does have deficiencies at low VOC:NO_x ratios. The scheme is as follows:

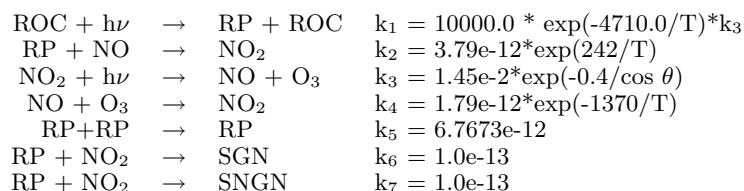


Table 1. The Generic Reaction Set. Molecule cm s units.

ROC represents reactive organic compounds, RP represents the radical pool while SGN and SNGN represent the stable gaseous and non-gaseous nitrogen products, respectively. The surrogate species ROC was made up from the inventory of VOC compounds, given in [19]. Each species, in [19], was assigned to a class according to their radical production reactivity. Each of these classes then had a reactivity coefficient allocated to it, as described in [20], which gave the final calculated quantity, \bar{a}_{ROC} . The ROC emissions were then calculated from the VOC emission rate multiplied by the scaling factor described. The rate of reaction for the ROC species was dependent on the photolysis rate of NO₂.

4.2 CBMLeeds

This scheme derived from the systematic reduction of the CBM-Ex[18], using a combination of sensitivity analysis and the application of the quasi-steady-state approximation (QSSA) across a range of initial conditions. The original CBM-Ex scheme consists of 90 species and 204 reactions, whereas the reduced CBMLeeds scheme contains 28 species and 59 reactions. The CBM-IV reduced mechanism, also by Gery *et al.*, has 33 species and 82 reactions, and has been used as one of the benchmarks against which both the GRS and CBMLeeds have been compared. After the reduction of CBM-Ex to CBMLeeds, there were 9 carbon bond species left to describe the VOCs: PAR (paraffin carbon bond), ETH (ethene), OLE (olefinic carbon bond), TOL (toluene), XYL (xylene), FORM (formaldehyde), ALD2 (high molecular weight aldehydes), KET (ketone carbonyl group) and ISOP (isoprene). Again, using the QUARG VOC speciation data [19], each VOC was broken down into its constituent parts, in a CBM context, so that the emissions could be speciated. The data for isoprene were not included in the simulations that follow. The CBMLeeds has been validated against CBM-Ex over a wide range of conditions, and consistently predicts O₃ concentrations to within 10%, which compares favourably with other reduced schemes such as CBM-IV.

5. Mesh generation and initial conditions

The following results were generated using a $500\text{km} \times 500\text{km}$ domain with the origin at OS Grid point (1500 E, 3000 N). The wind field had a constant velocity of 5 ms^{-1} in a northerly direction, and the eddy diffusion parameter was given a value of $300\text{ m}^2\text{s}^{-1}$, but because the ‘thin plume approximation’ is being used, the diffusion operator only works perpendicular to the direction of travel of the plume. The initial mesh had around 800 elements in each case, with the additional pre-refinement around the power station chimneys of most interest. In the Trent valley in Yorkshire, there are three coal-fired power stations in relatively close proximity, at Eggborough, Ferrybridge and Drax, which provide a range of interesting scenarios to investigate. The mesh was locally refined four levels, centred on each of the power stations, such that the elements nearest the source have length scales of less than 1km , which was necessary to cope with the steep spatial gradients of NO_x that arise in the vicinity of the concentrated source.

6. Results

Figure 2a shows the initial mesh for each calculation, while figure 2b shows the mesh for the level 2 adaptive solution shown in figure 3b. It should be noted that the meshes shown consist of a mixture of hexagons and pentagons, which are an artifact of the visualisation software, and have been created by connecting the centroids of adjacent triangles.

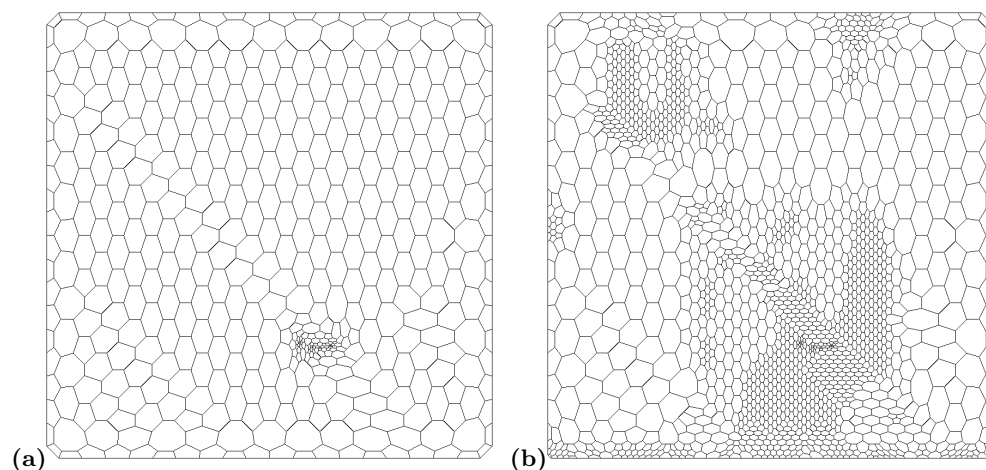


Figure 2. Difference in the meshes. The shapes shown are from joining centroids of adjoining triangles. (a) Initial mesh for both level 0 and level 2 simulations, showing pre-refinement about power stations. (b) Mesh for solution shown in Figure 3b.

The simulations were performed for a 48 hour period, starting at midnight of the first day, to monitor the diurnal variations in the ozone concentrations. The following contour plots (figures 3a and 3b) show the differences between simulations at different levels of adaptivity with both sets of data having been taken from 16:00 of the second day of the simulation. Figure 3a shows the level 0 non-adaptive solution while figure 3b shows the level 2 adaptive solution. It can be seen that the results shown in figure 3a only pick up the gross features of the solution, which are shown in more detail in figure 3b. Interestingly, the total ozone concentration, when summed across the whole domain, is quite similar in both simulations, but the local differences are quite marked, for example around Edinburgh and Glasgow, in the top right left hand corner of figures 3a and 3b.

Close to each of the point sources, as well as the larger urban sources, the level of the NO_x emissions inhibits the formation of ozone, by reaction 4 in Table 1. As the plumes travel downwind of the sources the background VOCs will mix in, which provide another route for NO to react, without the consumption of O_3 , leading to NO_2 . The photolysis of NO_2 , reaction 3 in Table 1, then reproduces O_3 , which can lead to raised O_3 concentrations, but only downwind of these sources.

With identical inputs at the southern (bottom) boundary, the difference in refinement in the mesh produces slightly different ozone concentrations by the time that the incoming air has reached the north

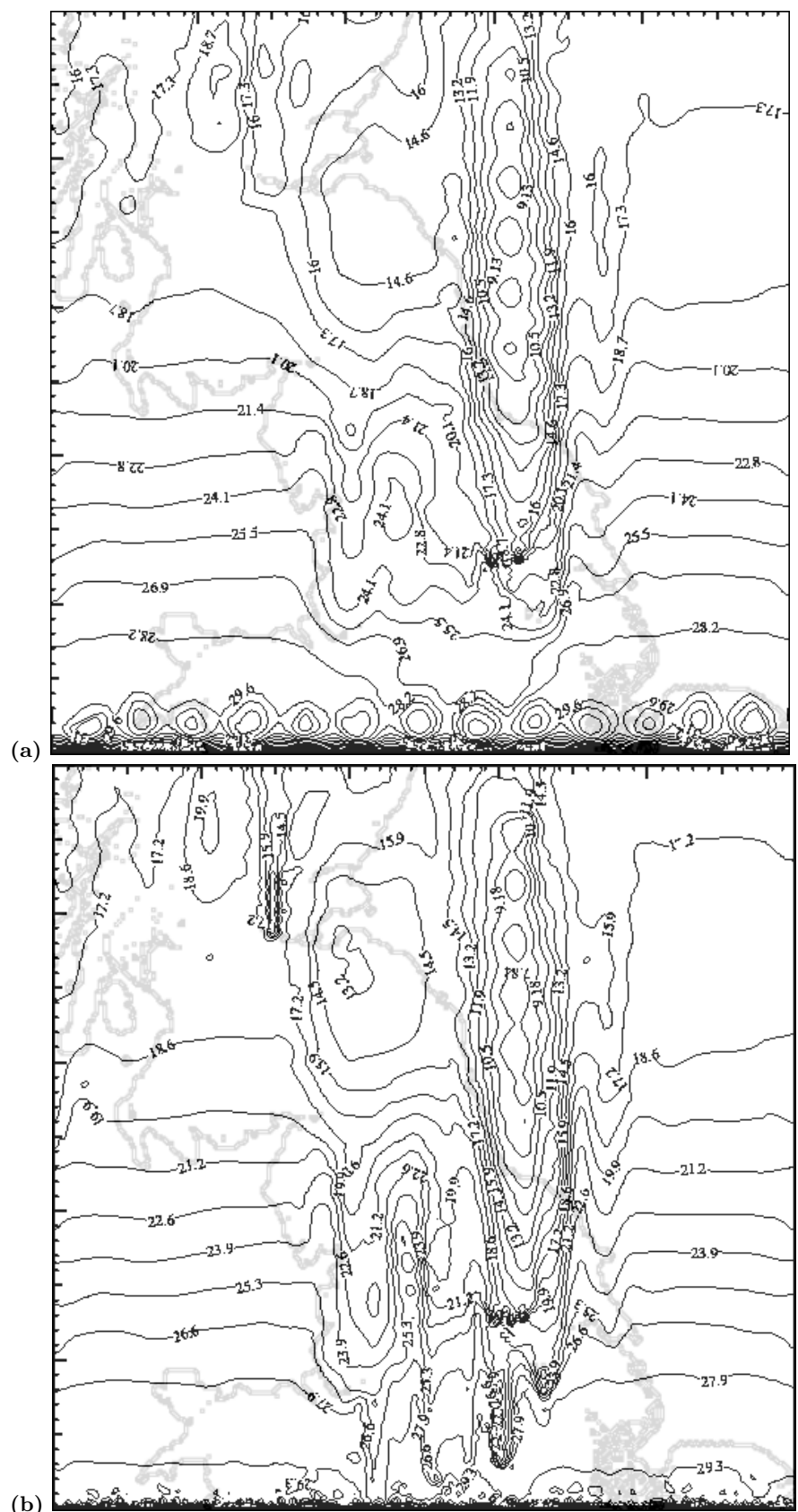


Figure 3. Ozone concentrations for a 500 x 500 km domain, covering northern area of UK. Contour values are in parts-per-billion (ppb), overlaid on the coastline. South - North runs from bottom to top.

of Wales, although only by less than 1 ppb. The initial refinement about the three power stations, which are about 100km north of the domain's southern boundary, helps give the power station plume more definition than it might have had otherwise, in the non-adaptive scenario, in which the urban plumes from Nottingham and Doncaster are barely discernible. The effects of the mixing in of these urban plumes is to reduce the ozone concentrations further in the mixed power station/urban plume, which continues out over the North Sea, which can be seen in the level 2 adaptive scenario.

The results for the non-adaptive run of the CBMLeeds scheme, which are not shown, reveal higher ozone concentrations off the east and west coasts of the UK as the air moves in from the southern boundary, as well as lower concentrations just up from the boundary. The higher regions can be attributed to the lack of NO_x over the seas, whereas the lower regions of ozone are probably due to differences in emission and deposition rates between the GRS and CBMLeeds models. This probably results from the better treatment given to VOC species in CBMLeeds, which were not accounted for fully in the model inputs. Owing to computer equipment failure, the results for a level 2 adaptive run could not be presented.

7. Discussion

The results shown above, as in [1], show that the adaptive mesh gridding techniques, used frequently in detonation modelling, can be applied to atmospheric reactive flow problems with promising results.

The GRS has been shown to be a useful tool for investigating scenarios rapidly, but it is also apparent that to get the results from the CBMLeeds scheme to match those of the GRS, more information about the inputs of the component CBM VOCs need to be input, since this appears to be the reason for the rapidly increased ozone levels. The CBMLeeds has been shown to perform very well, when modelling O_3 and it is hoped that this chemical scheme will provide the basis of the progression to a three dimensional model.

The errors in the computations on a fixed grid, that arise from the nonlinearities in the chemistry, can be minimised by allowing the meshes to refine where there are large errors. It has already been noted [21] that, because of the nonlinearities involved in the interdependence of the chemistry and the flow field, that the concentrations of the reactive species, especially the highly reactive radical intermediates, become mesh dependent.

The use of adaptive algorithms would appear to be a significant advance for regional air pollution models, and it is hoped that as computational capacity increases, the level of refinement possible can be increased. This will allow closer comparison with experimental field results, which will in turn hopefully lead to a better understanding of the complex processes that are going on.

8. References:

- 1: Tomlin, A., Berzins, M., Ware, J., Smith, J.D. and Pilling, M.J. Submitted to Atmospheric Environment (1996)
- 2: Derwent, R.G. and Jenkin, M.E., AERE-report **R13736** (1990)
- 3: Moussiopoulos, N. Eurotrac94 - ISS Garmisch-Partenkirchen (1994)
- 4: Jakobs, H.J. Eurotrac94 (1994)
- 5: Sunderman, S., Logan, J.A. and Wofsy, S.C., Journal of Geophysical Research, **95**, 5731, (1990)
- 7: Tomlin A., Ware, J., Smith, J., Berzins, M., Pilling, M. Air Pollution III - Computational Mechanics special publication, 201, (1995)
- 8: Berzins, M. and Ware, J.M. Applied Numerical Mathematics, **20**, 83, (1996)
- 9: Berzins, M., Dew, P. and Furzeland, R.M. Appl. Numer. Math., **5**, 375, (1989)
- 10: Berzins, M., Lawson, J. and Ware, J.M. In "Advances in Computer Methods for Partial Differential Equations VII", 60, (1992)
- 11: Berzins, M. SIAM J. Sci. Comp., **16**, 558, (1995)
- 12: Berzins, M. and Ware, J.M. Appl. Numer. Math., **16**, 417, (1995)
- 13: Berzins, M. and Furzeland, R.M. Appl. Numer. Math., **9**, 1, (1992)
- 14: Joe, B. and Simpson, R.B. Int. J. Numer. Meth. Eng., **23**, 987, (1991)
- 15: Derwent, R.G. and Jenkin, M.E., AERE-report **R13816** (1990)
- 16: Azzi, M., Johnson, G.M., and Cope, M. Proc. 11th Int. Clean Air Conference, 4th Regional IUPPA

Conf., Brisbane, Australia (1992)

17: Heard, A., Pilling, M.J., Tomlin, A. Submitted to Atmospheric Environment (1996)

18: Gery M.W., Whitten, G.Z., Killus, J.P. and Dodge, M.C. J. Geophys. Res., **94(D10)**, 12,925, (1989)

19: Quality of Urban Air Review Group (QUARG) First report (1993)

20: Venkatram, A, Karamchandani, P., Pai, P. and Goldstein, R. Atmospheric Environment **28**, 3665, (1994)

21: Jang, J-C. C., Jeffries, H.E., Byun, D. and Pleim, J.E. Atmospheric Environment, **29**, 3085, (1995)